Monthly Notices
of the
ROYAL ASTRONOMICAL SOCIETY

Mon. Not. R. Astron. Soc. **426,** 2758–2771 (2012) doi:10.1111/j.1365-2966.2012.21887.x

Stochastic backgrounds of gravitational waves from cosmological sources – the role of dark energy

Oswaldo D. Miranda★

INPE – Instituto Nacional de Pesquisas Espaciais, Divisão de Astrofísica, Av. dos Astronautas 1758, São José dos Campos, 12227-010 SP, Brazil

Accepted 2012 August 8. Received 2012 August 8; in original form 2010 January 11

ABSTRACT

In this work we investigate the detectability of the gravitational stochastic background produced by cosmological sources in scenarios of structure formation. The calculation is performed in the framework of hierarchical structure formation using a Press–Schechter-like formalism. The model considers the coalescences of three kinds of binary systems, namely double neutron stars (NS–NS), the neutron star–black hole (NS–BH) binaries and the black hole–black hole (BH–BH) systems. We also included in the model the core-collapse supernovae leaving black holes as compact remnants. In particular, we use two different dark energy scenarios, specifically cosmological constant (Λ) and Chaplygin gas, in order to verify their influence on the cosmic star formation rate, the coalescence rates and the gravitational wave backgrounds. We calculate the gravitational wave signals separately for each kind of source and also determine their collective contribution for the stochastic background of gravitational waves. Concerning the compact binary systems, we verify that these sources produce stochastic backgrounds with signal-to-noise ratio (S/N) values $\sim$1.5 ($\sim$0.90) for NS–NS, $\sim$0.50 ($\sim$0.30) for NS–BH, $\sim$0.20 ($\sim$0.10) for BH–BH and $\sim$0.14 ($\sim$0.07) for core-collapse supernovae for a pair of advanced LIGO detectors in the cosmological-constant (Chaplygin gas) cosmology. Particularly, the sensitivity of the future third-generation detectors such as the Einstein Telescope (ET), in the triangular configuration, could increase the present S/N values by a high factor ($\sim$300–1000) when compared to the S/N calculated for advanced LIGO detectors. As an example, the collective contribution of these sources can produce S/N $\sim$ 3.3 ($\sim$1.8) for the Λ (Chaplygin gas) cosmology for a pair of advanced LIGO interferometers and within the frequency range $\sim$10 Hz–1.5 kHz. Considering ET we have S/N $\sim$ 2200 ($\sim$1300) for the Λ (Chaplygin gas) cosmology. Thus, the third-generation gravitational wave detectors could be used to reconstruct the history of star formation in the Universe and to contribute for the characterization of the dark energy, for example, identifying if there is evidence for the evolution of the dark energy equation-of-state parameter $w(a)$.

Key words: gravitational waves – binaries: close – stars: neutron – cosmology: theory – dark energy – large-scale structure of Universe.

1 INTRODUCTION

The direct detection of gravitational waves (GWs) is a major challenge for physics/astrophysics and considerable experimental effort is being devoted by several groups around the world. In particular, the window in the frequency range $\sim$10–10 kHz is open due topioneering efforts of the following interferometers: LIGO detectors (e.g. Abbott et al. 2009), Virgo detector (e.g. Acernese et al. 2008), GEO 600 detector (e.g. Grote et al. 2008) and TAMA 300 detector (e.g. Takahashi et al. 2004).

In the future, another window in the low-frequency range $\sim 10^{-4}$ to 10 Hz will be open by space antennas such as *e-LISA/NGO* (Amaro-Seoane et al. 2012), *BBO* (Cutler & Harms 2006) and *DECIGO* (Ando et al. 2010). These interferometers together with ground-based detectors which are presently in project, such as KAGRA (Somiya 2012), and the third-generation resonant mass detectors, such as SCHENBERG (Aguiar et al. 2008) and MiniGRAIL (Gottardi et al. 2007), will transform the research in general relativity into an observational/theoretical study.

On the other hand, as GWs are produced by a large variety of astrophysical sources and cosmological phenomena, it is quite probable that the Universe is pervaded by a background of such waves. Collapse of Population II and III stars, phase transitions in the early

★E-mail: oswaldo@das.inpe.br

Universe, cosmic strings and a variety of binary stars are some examples of sources that could produce such a putative background of GWs (see e.g. de Araujo, Miranda & Aguiar 2000, 2002, 2004; Maggiore 2000; Regimbau & de Freitas Pacheco 2001; Miranda, de Araujo & Aguiar 2004; de Araujo & Miranda 2005; Sandick et al. 2006; Suwa et al. 2007; Giovannini 2009; Pereira & Miranda 2010, among others).

Observe that the indirect evidence for the existence of GWs first came from observations of the orbital decay of the Hulse–Taylor binary pulsar (Hulse & Taylor 1974, 1975a,b). In this century, direct detection and analysis of GW sources are expected to provide a unique insight to one of the least understood of the fundamental forces (Belczyński, Kalogera & Bulik 2002). Specifically, GWs could also be used as a tool for studying the viability of different alternative theories of gravity. This could be done by comparing the detected polarization modes with those predicted by general relativity (see e.g. de Paula, Miranda & Marinho 2004; Alves, Miranda & de Araujo 2009).

As mentioned above, a number of interferometers designed for GW detection are currently in operation, being developed or planned. In particular, the high-frequency part of the GW spectrum ($10\,\mathrm{Hz} \lesssim f \lesssim 10\,\mathrm{kHz}$) is open today through the pioneering efforts of the first-generation ground-based interferometers such as LIGO. While detections from these first-generation detectors are likely to be rare, the third-generation GW detectors such as the Einstein Telescope (ET) may detect, among others, the stochastic signal generated by a population of pre-galactic stars. Thus, GW observations could add a new dimension to our ability to observe and understand the Universe.

On the other hand, the state of the art in cosmology has led to the following distribution of the energy densities of the Universe: 4 per cent for baryonic matter, 23 per cent for non-baryonic dark matter and 73 per cent for the so-called dark energy (Jarosik et al. 2011). Concerning the dark energy, some equations of state have been proposed in order to explain such a dark component. The most common example is the cosmological constant [cold dark matter (ΛCDM) model], which implies a constant vacuum energy density along the history of the Universe. Another possibility is a dynamical vacuum or quintessence. In general, the quintessence models involve one (Albrecht & Skordis 2000) or two (Bento, Bertolami & Santos 2002) coupled scalar fields. The Chaplygin gas is another example of dark energy fluid. One of the most appealing aspects of the original Chaplygin gas model is that it is equivalent to the Dirac–Born–Infeld description of a Nambu–Goto membrane (Bordemann & Hoppe 1994; Gorini et al. 2005; Ogawa 2010).

In this way, the main goal of the present work is to explore the possibility of using stochastic backgrounds of GWs to provide more information about the character and interrelationship of the dark energy equation of state and the star formation at high redshifts. That is, in the first place we analyse the influence of two different dark energy components of the Universe, namely cosmological constant and Chaplygin gas, on the stochastic backgrounds of GWs produced by four different cosmological sources – the merging together of two neutron stars (NS–NS), the coalescence of neutron star and black hole (NS–BH) systems, the merger of two black holes (BH–BH) and the core-collapse supernovae (SNe) leaving black holes as compact remnants. Secondly, we show that different dark energy fluids produce distinct signatures for the cosmic star formation rate (CSFR) especially at high redshifts ($z > 3$). This interesting feature could be used as an alternative way to study the star formation and the possible temporal dependence of the dark energy equation of state up to redshift 20, having as the common tool a stochastic background of GWs with high signal-to-noise ratio (S/N). In this way, not only binary systems at lower redshifts ($z < 2$–3) working as standard sirens but also stochastic backgrounds of GWs could contribute for a better comprehension of the physical nature of the dark energy and their connection, and influence the star formation at high redshifts.

The preference for concentrating attention on the Chaplygin gas also comes from recent work of Pace, Waizmann & Bartelmann (2010), who analysed the spherical collapse model in dark energy cosmologies. As can be seen from that work, the Chaplygin gas exhibits an equation of state dependent on time as the quintessence models also exhibit. It is not the purpose of the present study to make an individual assessment of each particular type of dark energy candidate. Our goal is to verify if stochastic backgrounds of GWs can give us some indication about the evolution of the dark energy equation of state with time. Thus, the comparison between Chaplygin gas and ΛCDM is sufficient for the purposes of this study.

Here, we start with the CSFR recently derived by Pereira & Miranda (2010). Specifically, these authors use a hierarchical structure formation model and they obtain the CSFR in a self-consistent way. This means that the authors solve the equation governing the total gas density taking into account the baryon accretion rate, treated as an infall term, and the lifetime of the stars formed in the dark matter haloes. Here, we adapted the formalism derived by Pereira & Miranda (2010) in order to obtain the CSFR and the coalescence rates consistent with the assumed dark energy model.

The paper is organized as follows. In Section 2, we review the basics of the hierarchical model and how to obtain the CSFR up to redshift $z \sim 20$ as a function of the specific dark energy cosmology. In Section 3, we discuss how to obtain the coalescence rates for NS–NS, NS–BH and BH–BH systems from the CSFR. In Section 4, we present the formalism used to characterize the GW backgrounds for compact binary systems and core-collapse SNe to form black holes. We also present the S/N values for both a pair of advanced LIGO detectors and the ET in triangular configuration. Section 5 presents the collective contribution of these sources for the GW background. In Section 6, we discuss the influence of the uncertainties of the parameters on the derived GW background and on the CSFR. Section 7 presents the final considerations of this work.

2 THE COSMIC STAR FORMATION RATE AND THE DARK ENERGY COSMOLOGIES

2.1 An overview

The essence of the halo model was discussed by Neyman, Scott & Shane (1952), who postulated that all galaxies form in clusters, the distribution of galaxies within clusters can be described by a probabilistic relation and cluster centres are themselves correlated. Substituting the word 'clusters' by 'haloes' in the paper of Neyman et al. (1952), we arrive at a reasonable qualitative description of the modern halo model. Today, it is widely believed that haloes, or overdense dark matter clumps, form as a result of the growth and non-linear evolution of density perturbations produced in the early Universe (Peacock 1999). This is the heart of the hierarchical formation scenario.

In general, the halo mass function is represented as the differential number density of haloes with mass between M and $M + \mathrm{d}M$. Press and Schechter (hereafter PS) heuristically derived a mass function for bound virialized objects in 1974 (Press & Schechter 1974).

The basic idea of the PS approach is to define haloes as concentrations of mass, which have already left the linear regime by crossing the threshold δ_c for non-linear collapse. Given a power spectrum and a window function, it should then be relatively straightforward to calculate the halo mass function as a function of the mass and redshift.

However, it is worth stressing that the exact definition of the mass function, e.g. integrated versus differential form or count versus number density, varies widely in the literature. To characterize different fits, the scale differential mass function $f(\sigma, z)$ (Jenkis et al. 2001) can be introduced, which is defined as a fraction of the total mass per $\ln \sigma^{-1}$ that belongs to haloes:

$$f(\sigma, z) \equiv \frac{\mathrm{d}\rho/\rho_\mathrm{B}}{\mathrm{d}\ln\sigma^{-1}} = \frac{M}{\rho_\mathrm{B}(z)} \frac{\mathrm{d}n(M,z)}{\mathrm{d}\ln[\sigma^{-1}(M,z)]}, \quad (1)$$

where $n(M, z)$ is the number density of haloes with mass M and $\rho_\mathrm{B}(z)$ is the background density at redshift z. As pointed out by Jenkis et al. (2001), this definition of the mass function has the advantage that it does not explicitly depend on redshift, power spectrum or cosmology; all of these are contained in $\sigma(M, z)$ (see also Lukić et al. 2007). Note that

$$\sigma(M, z) = \sigma(M, z = 0)D(z) \quad (2)$$

is the linear rms density fluctuation in spheres of comoving radius R containing the mass M and $D(z)$ is the linear growth function.

The density of baryons is proportional to the density of dark matter if we consider that the baryon distribution traces the dark matter. Thus, the fraction of baryons at redshift z that are in structures is given by (see e.g. Daigne et al. 2006; Pereira & Miranda 2010)

$$f_\mathrm{b}(z) = \frac{\int_{M_\mathrm{min}}^{M_\mathrm{max}} f(\sigma) M \mathrm{d}M}{\int_0^\infty f(\sigma) M \mathrm{d}M}, \quad (3)$$

where we have used $M_\mathrm{min} = 10^6\,\mathrm{M}_\odot$ and $M_\mathrm{max} = 10^{18}\,\mathrm{M}_\odot$ (see Pereira & Miranda 2010 for details).

Therefore, the baryon accretion rate $a_\mathrm{b}(t)$ which accounts for the increase in the fraction of baryons in structures is given by

$$a_\mathrm{b}(t) = \Omega_\mathrm{b}\rho_\mathrm{c} \left(\frac{\mathrm{d}t}{\mathrm{d}z}\right)^{-1} \left|\frac{\mathrm{d}f_\mathrm{b}(z)}{\mathrm{d}z}\right|, \quad (4)$$

where $\rho_\mathrm{c} = 3H_0^2/8\pi G$ is the critical density of the Universe.

The age of the Universe that appears in (4) is related to the redshift by

$$\frac{\mathrm{d}t}{\mathrm{d}z} = \frac{9.78\,h^{-1}\,\mathrm{Gyr}}{(1+z)E(z)}. \quad (5)$$

In equation (5), $E(z)$ represents the expansion function which is given by (see e.g. Pace et al. 2010)

$$E(z) = \sqrt{\Omega_\mathrm{m}(1+z)^3 + \Omega_\mathrm{d} \exp\left(-3\int_1^a \frac{1+w(a')}{a'}\mathrm{d}a\right)}, \quad (6)$$

where the relative density of the i-component is given by $\Omega_\mathrm{i} = \rho_\mathrm{i}/\rho_\mathrm{c}$; here 'i' applies for baryons (b), dark energy (d) and total matter (m). As usual, the scale factor is $a = 1/(1+z)$, and $w(a)$ is the dark energy equation-of-state parameter.

Note that for $w(a) = -1$ we have the equation-of-state parameter of the cosmological constant. In this case,

$$E(z) = \sqrt{\Omega_\mathrm{m}(1+z)^3 + \Omega_\Lambda}, \quad (7)$$

with $\Omega_\mathrm{d} = \Omega_\Lambda$.

The linear growth function, in equation (2), is defined as $D(z) \equiv \delta_\mathrm{m}(z)/\delta_\mathrm{m}(z=0)$ and is obtained as a solution from the following equation (see Pace et al. 2010, for details):

$$\delta_\mathrm{m}'' + \left(\frac{3}{a} + \frac{E'}{E}\right)\delta_\mathrm{m}' - \frac{3}{2}\frac{\Omega_\mathrm{m}}{a^5E^2}\delta_\mathrm{m} = 0, \quad (8)$$

where the derivatives are taken in relation to the scale factor a.

On the other hand, the equation governing the total gas mass (ρ_g) in the haloes is

$$\dot{\rho}_\mathrm{g} = -\frac{\mathrm{d}^2M_\star}{\mathrm{d}V\mathrm{d}t} + \frac{\mathrm{d}^2M_\mathrm{ej}}{\mathrm{d}V\mathrm{d}t} + a_\mathrm{b}(t). \quad (9)$$

The first term on the right-hand side of equation (9) represents the stars which are formed by the gas contained in the haloes. Using a Schmidt law (Schmidt 1959, 1963), we can write for the star formation rate

$$\frac{\mathrm{d}^2M_\star}{\mathrm{d}V\mathrm{d}t} = \Psi(t) = k\rho_\mathrm{g}(t), \quad (10)$$

where k is the inverse of the time-scale for star formation, i.e. $k = 1/\tau_\mathrm{s}$.

The second term on the right-hand side of equation (9) considers the mass ejected from stars through winds and SNe. Therefore, this term represents the gas which is returned to the 'interstellar medium of the system'. Thus, we can write (see e.g. Tinsley 1973)

$$\frac{\mathrm{d}^2M_\mathrm{ej}}{\mathrm{d}V\mathrm{d}t} = \int_{m(t)}^{140\,\mathrm{M}_\odot} (m - m_\mathrm{r})\Phi(m)\Psi(t - \tau_\mathrm{m})\,\mathrm{d}m, \quad (11)$$

where the limit $m(t)$ corresponds to the stellar mass whose lifetime is equal to t. In the integrand, m_r is the mass of the remnant, which depends on the progenitor mass (see Tinsley 1973 for details), and the star formation rate is taken at the retarded time $(t - \tau_\mathrm{m})$, where τ_m is the lifetime of a star of mass m.

For all stars formed in the haloes, the metallicity-independent fit of Scalo (1986) and Copi (1997) is used:

$$\log_{10}(\tau_\mathrm{m}) = 10.0 - 3.6\,\log_{10}\left(\frac{M}{\mathrm{M}_\odot}\right) + \left[\log_{10}\left(\frac{M}{\mathrm{M}_\odot}\right)\right]^2, \quad (12)$$

where τ_m is the stellar lifetime given in years.

In equation (11), the term $\Phi(m)$ represents the initial mass function (IMF) which gives the distribution function of stellar masses. Thus,

$$\Phi(m) = Am^{-(1+x)}, \quad (13)$$

where x is the slope of the IMF, and A is a normalization factor determined by

$$\int_{0.1\,\mathrm{M}_\odot}^{140\,\mathrm{M}_\odot} m\Phi(m)\,\mathrm{d}m = 1. \quad (14)$$

Numerical integration of (9) produces the function $\rho_\mathrm{g}(t)$ at each time t (or redshift z). Once $\rho_\mathrm{g}(t)$ is obtained, we return to equation (10) in order to obtain the CSFR. Just replacing $\Psi(t)$ by $\dot{\rho}_\star(t)$, we have

$$\dot{\rho}_\star = k\rho_\mathrm{g}. \quad (15)$$

It is worth stressing that although we did not take into account the stellar feedback processes on the derivation of the CSFR (see e.g. Christensen et al. 2010, for this issue), our models, as we will discuss below, have a good agreement with observational data taken from Hopkins (2004, 2007) at lower redshifts ($z < 5$). Furthermore, the CSFR obtained in the present work has a good agreement with the one derived by Springel & Hernquist (2003) from hydrodynamic simulations. Regardless, we should comment on this limitation of the model in its present form. In particular, stellar feedback processes can modify the time-scale (τ_s) for star formation, for example, through radiation, winds and SN events from massive stars.

As a main result, the star formation efficiency, $\varepsilon_\star$, embedded in the normalization of the CSFR at $z = 0$ (see Pereira & Miranda 2010, for this issue), and τ_s would be functions of time. In principle, τ_s and $\varepsilon_\star$, which are not constants, can modify the shape of the CSFR at higher redshifts. On the other hand, due to the good agreement with observations at $z < 2$, where data are less scattered, the values used in this work should represent reasonable mean values of these quantities over the whole interval $[0, z_{ini}]$. Certainly, the inclusion of stellar feedback processes would be an interesting refinement to introduce in future works.

2.2 The dark energy models and the input parameters

The last point we have to consider for the characterization of the CSFR is the dark energy component of the Universe through its equation-of-state parameter $w(a)$. In the present work, we consider two cases: cosmological constant where $w(a) = -1$ and the Chaplygin gas.

In particular, the Chaplygin gas is characterized by a fluid with an equation of state $p = -A/\rho^\alpha$. This dark energy fluid has been tested against observational data such as Type Ia SN (SNIa; e.g Colistete & Fabris 2005), cosmic microwave background (e.g. Piattella 2010) and power spectrum (e.g. Fabris, Velten & Zimdahl 2010), and it configures in a strong alternative candidate to the cosmological constant.

Its equation-of-state parameter is given by

$$w(a) = -\frac{A}{A + B\,a^{-3(\alpha+1)}}. \tag{16}$$

In equation (16), the constants A and B are (see e.g. Pace et al. 2010 for details)

$$A = -w_0(\Omega_d\rho_c)^{1+\alpha} \quad \text{and} \quad B = (1 + w_0)(\Omega_d\rho_c)^{1+\alpha}. \tag{17}$$

The present value of the equation-of-state parameter is related to A and B by

$$w_0 = -\frac{A}{A + B}. \tag{18}$$

The cosmological parameters we have used in this work are $\Omega_d = 0.762$, $\Omega_m = 0.238$, $\Omega_b = 0.042$ and Hubble constant $H_0 = 100\,h\,\mathrm{km\,s^{-1}\,Mpc^{-1}}$, with $h = 0.734$. For the variance of the overdensity field smoothed on a scale of size $8\,h^{-1}$ Mpc, we consider $\sigma_8 = 0.8$. The parameters associated with the Chaplygin gas are $\alpha = 1.0$ (classical Chaplygin gas) and $\alpha = 0.2$ (generalized version). In both cases we consider $w_0 = -0.8$.

In column 1 of Table 1 is shown the name of the models. In column 2, we present the slope of the IMF (x in equation 13); the time-scale for star formation is presented in column 3, the redshift (z_p) where the CSFR peaks is presented in column 4 and finally, in column 5, we have the kind of dark fluid.

All models presented in Table 1 have a good agreement with observational data. In particular, χ^2 analysis was performed over these models, obtaining the reduced χ^2 defined as $\chi_r = \chi^2/\mathrm{d.o.f.}$ (where 'd.o.f.' means 'degrees of freedom'). All of these models satisfy $\chi_r < 1$. In Fig. 1, we present the CSFR derived from equation (15) for three models of Table 1. The observational points are taken from Hopkins (2004, 2007).

We can see from the results in Table 1 and Fig. 1 that the cosmological constant produces amplitudes higher than that produced by the Chaplygin gas. This means that the process of baryonic matter infall from the haloes is more efficient, for the same set of parameters, if the dark energy fluid is the cosmological constant. Another characteristic which can be seen from Fig. 1 and Table 1 is that the Chaplygin gas decreases the redshift where the CSFR peaks when compared to the cosmological constant.

Table 1. The input parameters used to obtain the CSFR. All CSFRs have a good agreement with observational data. The redshift z_{ini} associated with the beginning of star formation is 20. In the fifth column, Λ represents the cosmological constant and α represents the Chaplygin gas.

CSFR	x (IMF)	τ_s (Gyr)	z_p	Dark fluid
A1	1.35	2.0	3.54	Λ
A2	1.35	3.0	2.94	Λ
A3	0.35	1.0	3.29	Λ
A4	1.35	2.0	2.75	$\alpha = 0.2$
A5	1.35	3.0	2.21	$\alpha = 0.2$
A6	0.35	1.0	2.52	$\alpha = 0.2$
A7	1.35	2.0	2.42	$\alpha = 1.0$
A8	1.35	3.0	1.91	$\alpha = 1.0$
A9	0.35	1.0	2.21	$\alpha = 1.0$

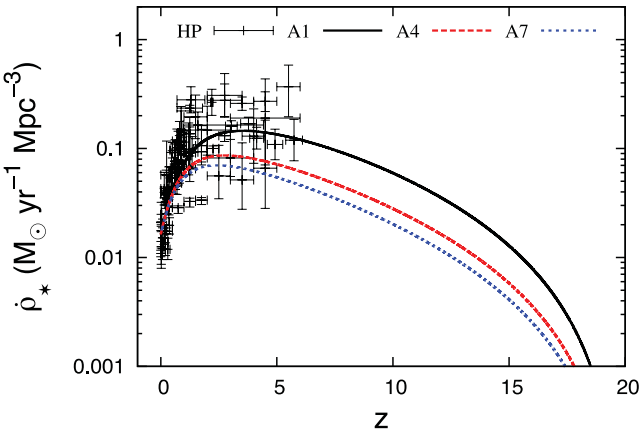

Figure 1. The CSFR derived in this work compared to the observational points (HP) taken from Hopkins (2004, 2007). The models are described in Table 1.

3 THE COALESCENCE RATES

We assume that the coalescence rates track the CSFR but with a delay t_d between the formation of the binary system and the final merger (see Regimbau & Hughes 2009). Thus, we can write

$$\dot{\rho}_c^0(z) = \dot{\rho}_c^0(0) \times \frac{\dot{\rho}_{\star c}(z)}{\dot{\rho}_{\star c}(0)}, \tag{19}$$

where $\dot{\rho}_c^0(z)$ is the rate at which binary systems are observed to merger at redshift z, and $\dot{\rho}_c^0(0)$ is the same rate in our local Universe.

The connection between the past CSFR and the rate of binary merger is given by $\dot{\rho}_{\star c}(z)$ through the relation

$$\dot{\rho}_{\star c}(z) = \int_{\tau_0}^{t(z)} \frac{\dot{\rho}_\star(z_f)}{(1 + z_f)} P(t_d)\,\mathrm{d}t_d, \tag{20}$$

where $\dot{\rho}_\star(z_f)$ is the CSFR obtained from equation (15), $P(t_d)$ is the probability per unit time of merging after the formation of the progenitor, including both the evolutionary time for the formation of the compact binary and the time for the compact binary to coalesce, and the $(1 + z_f)$ term in the denominator considers the time dilatation due to the cosmic expansion.

The time delay $t_{\rm d}$ makes the connection between the redshift z at which a compact binary system merges and the redshift $z_{\rm f}$ at which its progenitor was formed. As discussed by Regimbau & Hughes (2009), it can be calculated as

$$t_{\rm d} = \frac{1}{H_0}\int_z^{z_{\rm f}} \frac{{\rm d}z'}{(1+z')E(z')}. \tag{21}$$

The probability $P(t_{\rm d})$ is described in the form

$$P(t_{\rm d}) \propto \frac{1}{t_{\rm d}}. \tag{22}$$

As mentioned in Regimbau & Hughes (2009), this form accounts for the wide range of merger times observed in binary pulsars. This form was also used by de Freitas Pacheco (1997), Regimbau & de Freitas Pacheco (2006) and de Freitas Pacheco et al. (2006) in their works. Thus, we define $P(t_{\rm d})$ as

$$P(t_{\rm d}) = \frac{B}{t_{\rm d}}, \tag{23}$$

where B is a normalization constant, and the probability function $P(t_{\rm d})$ is normalized in the range τ_0–15 Gyr for some minimal delay τ_0. Therefore,

$$\int_{\tau_0}^{15{\rm Gyr}} \frac{B}{t_{\rm d}}{\rm d}t_{\rm d} = 1. \tag{24}$$

Specifically, we consider that $\tau_0 = 20$ Myr for NS–NS systems, $\tau_0 = 10$ Myr for NS–BH systems and $\tau_0 = 100$ Myr for BH–BH systems (Bulik, Belczyński & Rudak 2004).

With these assumptions, the merger rate per unit redshift can be written as

$$\frac{{\rm d}R_{\rm c}^0}{{\rm d}z} = \dot{\rho}_{\rm c}^0(z)\frac{{\rm d}V}{{\rm d}z}, \tag{25}$$

where ${\rm d}V$ is the comoving volume element given by

$${\rm d}V = 4\pi r(z)^2 \frac{c}{H_0}\frac{{\rm d}z}{E(z)}. \tag{26}$$

In equation (26), $r(z)$ is the proper distance, whose expression is

$$r(z) = \frac{c}{H_0}\int_0^z \frac{{\rm d}z}{E(z)}. \tag{27}$$

Note that the expansion function $E(z)$ is dependent on the kind of dark energy fluid as shown by equation (6). Then, using the formalism described in this section, the cosmic coalescence rates for NS–NS binaries, NS–BH and BH–BH systems up to redshift $z \sim 20$ can be determined. Fig. 2 presents the cosmic coalescence rates, normalized to the local value $\dot{\rho}_{\rm c}^0(0)$, for NS–NS binaries. On the other hand, Figs 3 and 4, respectively, show the cosmic coalescence rates for NS–BH and BH–BH binaries.

As expected, due to the behaviour of the CSFR, the amplitudes of the coalescence rates produced by the Chaplygin gas cosmology are lower than those produced by the cosmological-constant cosmology. In particular, for the cosmological constant (model A1), $\dot{\rho}_{\rm c}^0(z)/\dot{\rho}_{\rm c}^0(0)$ reaches a maximum amplitude at redshift $z = 2.27$ for NS–NS binaries, at $z = 2.45$ for NS–BH and at $z = 1.86$ for BH–BH systems. In the case of generalized Chaplygin gas ($\alpha = 0.2$ – model A4), we note that $\dot{\rho}_{\rm c}^0(z)/\dot{\rho}_{\rm c}^0(0)$ peaks at $z = 1.63$ for NS–NS, at $z = 1.81$ for NS–BH and at $z = 1.31$ for BH–BH. The last case, classical Chaplygin gas ($\alpha = 1.0$), reaches a maximum amplitude at $z = 1.34$ for both NS–NS and NS–BH systems. On the other hand, for BH–BH binaries the maximum value of the coalescence rate is reached at $z = 1.13$. Thus, the position of the peak of the coalescence rate is dictated by the value of τ_0 and also by the kind of dark energy fluid.

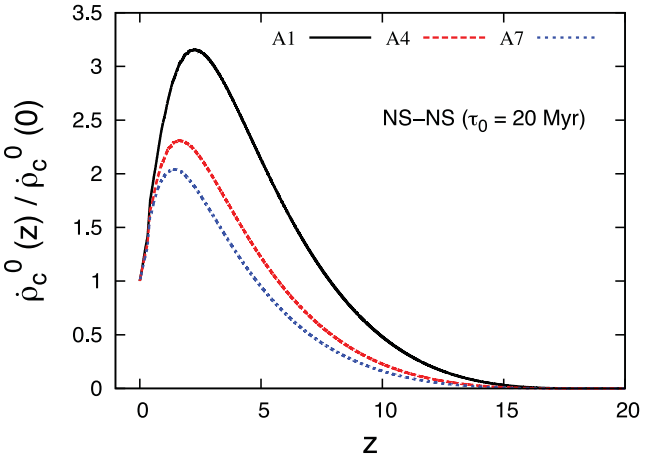

Figure 2. The cosmic coalescence rates for NS–NS binaries. The models consider $\tau_0 = 20$ Myr. These models are obtained from the CSFR presented in Fig. 1 (see also Table 1 for the main parameters).

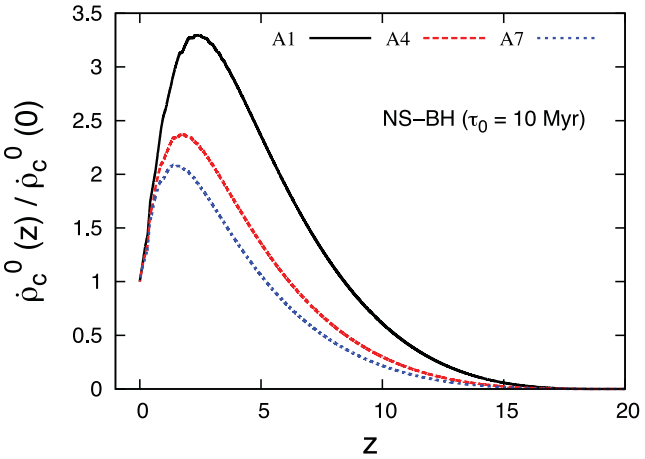

Figure 3. The cosmic coalescence rates for NS–BH binaries. The models consider $\tau_0 = 10$ Myr. These models are obtained from the CSFR presented in Fig. 1 (see also Table 1 for the main parameters).

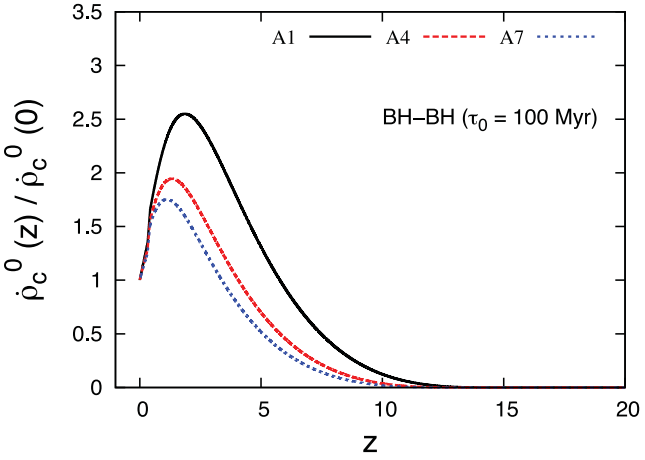

Figure 4. The cosmic coalescence rates for BH–BH binaries. The models consider $\tau_0 = 100$ Myr. These models are obtained from the CSFR presented in Fig. 1 (see also Table 1 for the main parameters).

As we will see in the next section, the different behaviours for the coalescence rates produced by different dark energy cosmologies will produce different values for the S/N of advanced LIGO and ET.

4 GRAVITATIONAL WAVE BACKGROUND

4.1 Compact binary systems

The spectrum of a stochastic background of GWs is characterized by the closure energy density per logarithmic frequency spam, which is given by (see e.g. Allen 1997; Allen & Romano 1999)

$$\Omega_{\rm GW} = \frac{1}{\rho_{\rm c}} \frac{{\rm d}\rho_{\rm GW}}{{\rm d}\log\ \nu_{\rm obs}}, \tag{28}$$

where $\rho_{\rm GW}$ is the gravitational energy density and $\nu_{\rm obs}$ is the frequency in the observer frame.

The above equation can be written as (see e.g. Ferrari, Matarrese & Schneider 1999)

$$\Omega_{\rm GW} = \frac{1}{c^3 \rho_{\rm c}} \nu_{\rm obs} F_{\nu_{\rm obs}}, \tag{29}$$

where $F_{\nu_{\rm obs}}$ is the GW flux (given in erg cm^{-2} Hz^{-1} s^{-1}) at the observer frequency $\nu_{\rm obs}$ integrated over all cosmological sources. Therefore,

$$F_{\nu_{\rm obs}} = \int_0^{z_{\rm ini}} f_{\nu_{\rm obs}}\, {\rm d}R_{\rm c}^0(z). \tag{30}$$

Note that ${\rm d}R_{\rm c}^0(z)/{\rm d}z$ is the merger rate per unit redshift (equation 25). In order to solve equation (30), the GW fluence ($f_{\nu_{\rm obs}}$), in the observer frame, produced by a given compact binary coalescence needs to be determined. Following Regimbau & de Freitas Pacheco (2006), Regimbau (2011), Regimbau et al. (2012), Zhu et al. (2011), Marassi et al. (2011a), Rosado (2011) and Wu, Mandic & Regimbau (2012), $f_{\nu_{\rm obs}}$ can be written as

$$f_{\nu_{\rm obs}} = \frac{1}{4\pi d_{\rm L}^2} \frac{{\rm d}E_{\rm GW}}{{\rm d}\nu} (1+z)^2, \tag{31}$$

where $d_{\rm L} = r(z)(1+z)$ is the luminosity distance, $r(z)$ is the proper distance (see equation 27), ${\rm d}E_{\rm GW}/{\rm d}\nu$ is the spectral energy and $\nu = \nu_{\rm obs}(1+z)$ is the frequency in the source frame.

In the quadrupolar approximation, the spectral energy emitted by a compact binary system, with masses m_1 and m_2, which inspirals in a circular orbit is given by (Peters & Mathews 1963)

$$\frac{{\rm d}E_{\rm GW}}{{\rm d}\nu} = K\, \nu^{-1/3}, \tag{32}$$

where

$$K = \frac{(G\pi)^{2/3}}{3} \frac{m_1 m_2}{(m_1+m_2)^{1/3}}. \tag{33}$$

It will be considered that the GW background has the value of the maximum frequency limited by the 'last stable orbit' (LSO). Then, following Sathyaprakash (2001),

$$\nu_{\rm max} = \nu_{\rm LSO} = 1.5 \left(\frac{M}{2.8\,{\rm M}_\odot}\right)^{-1} {\rm kHz}, \tag{34}$$

where M is the total mass of the system ($M = m_1 + m_2$).

In the present study, we consider $m_1 = m_2 = 1.4\,{\rm M}_\odot$ for NS–NS binaries, while for NS–BH we used $m_1 = 1.4\,{\rm M}_\odot$ and $m_2 = 7.0\,{\rm M}_\odot$. For BH–BH systems, we have used $m_1 = m_2 = 7.0\,{\rm M}_\odot$. With these considerations, the maximum frequency is $\nu_{\rm LSO} = 1.5$ kHz (500 Hz) for NS–NS (NS–BH). For BH–BH binaries, we have $\nu_{\rm LSO} = 300$ Hz.

There is one last point to consider before calculating the spectrum of the stochastic background of GWs. This point is related to the value of the local merger rate per unit volume, $\dot{\rho}_{\rm c}^0(0)$. As discussed by Regimbau & Hughes (2009), the local merger is usually extrapolated by multiplying the rate in the Milky Way with the density of equivalent galaxies.

Current estimates give $\dot{\rho}_{\rm c}^0(0) = (0.01\text{–}10)\,{\rm Myr}^{-1}\,{\rm Mpc}^{-3}$ for NS–NS and $\dot{\rho}_{\rm c}^0(0) = (0.001\text{–}1)\,{\rm Myr}^{-1}\,{\rm Mpc}^{-3}$ for NS–BH (see Regimbau & Hughes 2009, and references therein). In the present work, it is considered $\dot{\rho}_{\rm c}^0(0) = 1.0\,{\rm Myr}^{-1}\,{\rm Mpc}^{-3}$ for NS–NS, $\dot{\rho}_{\rm c}^0(0) = 0.1\,{\rm Myr}^{-1}\,{\rm Mpc}^{-3}$ for NS–BH and $\dot{\rho}_{\rm c}^0(0) = 0.01\,{\rm Myr}^{-1}\,{\rm Mpc}^{-3}$ for BH–BH.

Thus, using the formalism above, we can obtain the characterization of the stochastic background of GWs formed by the coalescence of compact binary systems. In particular, Figs 5–7 present the spectra of the gravitational energy density parameter $\Omega_{\rm GW}$ versus the observed frequency $\nu_{\rm obs}$.

The density parameter increases as $\nu_{\rm obs}^{2/3}$ at low frequencies and reaches a maximum amplitude $\sim 3.8 \times 10^{-9}$ around 375 Hz for NS–NS systems if the CSFR-A1 (cosmological constant) is used. It is worth stressing that calculations performed by Regimbau & de Freitas Pacheco (2006), using Monte Carlo methods for obtaining the coalescence rates, produced similar results.

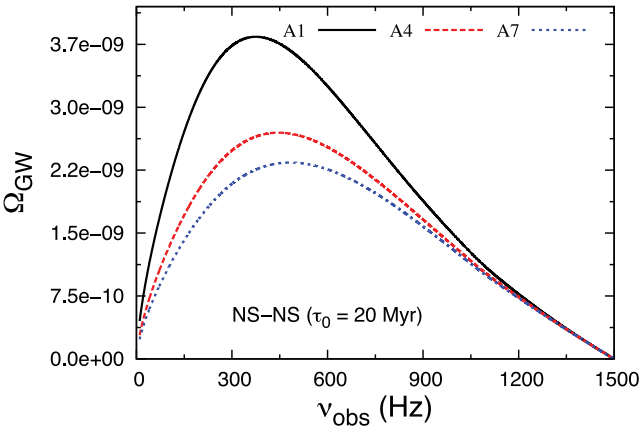

Figure 5. Spectrum of the gravitational energy density parameter $\Omega_{\rm GW}$. The results are shown for double neutron stars (NS–NS).

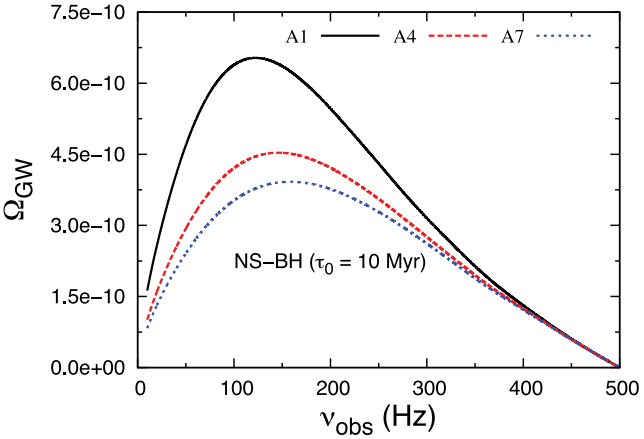

Figure 6. Spectrum of the gravitational energy density parameter $\Omega_{\rm GW}$. The results are shown for the coalescence of neutron star and black hole (NS–BH) systems.

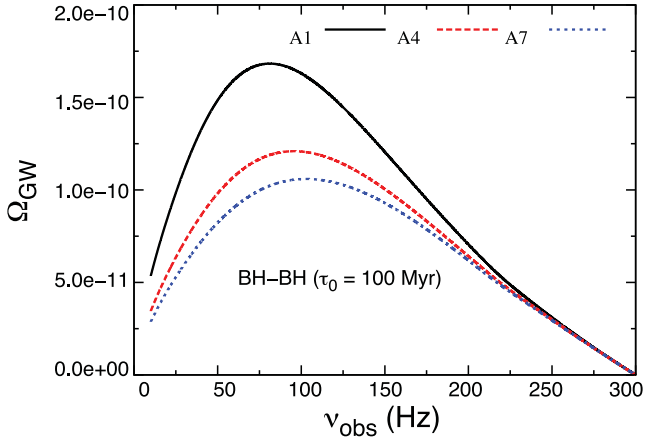

Figure 7. Spectrum of the gravitational energy density parameter Ω_{GW}. The results are shown for the coalescence of black hole–black hole (BH–BH) systems.

In particular, these authors obtained maximum amplitude of about 1.1×10^{-9} around 670 Hz for NS–NS binaries (considering their fiducial CSFR). However, observing the distribution of coalescences as a function of the redshift derived by Regimbau & de Freitas Pacheco (2006), we note that it peaks at $z \sim 1.5$. On the other hand, our coalescence rates peak at $z \sim 2.9$–3.5 (models A1–A3 which correspond to the cosmological constant as dark fluid). In this way, the maximum value of Ω_{GW} is shifted to lower frequency than that obtained by Regimbau & de Freitas Pacheco (2006).

In order to assess the detectability of a GW signal, one must evaluate the S/N, which for a pair of interferometers is given by (seee.g. Christensen 1992; Flanagan 1993; Allen 1997; de Araujo et al. 2002, 2004; Regimbau & de Freitas Pacheco 2006)

$$(\mathrm{S/N})^2 = \left[\left(\frac{9H_0^4}{50\pi^4}\right) T \int_0^\infty \mathrm{d}\nu \frac{\gamma^2(\nu)\Omega_{GW}^2(\nu)}{\nu^6 S_h^{(1)}(\nu) S_h^{(2)}(\nu)}\right], \quad (35)$$

where $S_h^{(i)}$ is the spectral noise density, T is the integration time and $\gamma(\nu)$ is the overlap reduction function, which depends on the relative positions and orientations of the two interferometers. For the $\gamma(\nu)$ function, we refer the reader to Flanagan (1993), who was the first to calculate a closed form for the LIGO observatories.

The noise power spectral density of the advanced LIGO can be found at LIGO website. However, we used here the analytical fit given by Mishra et al. (2010). Its expression is

$$S_h(\nu) = S_0 \left[10^{16-4(\nu-7.9)^2} + 2.4 \times 10^{-62}\, x^{-50} + 0.08\, x^{-4.69} + 123.35 \left(\frac{1 - 0.23\, x^2 + 0.0764\, x^4}{1 + 0.17\, x^2}\right)\right] \text{ if } \nu \geq \nu_s,$$
$$= \infty \text{ if } \nu < \nu_s, \quad (36)$$

where $x = \nu/\nu_0$, ν stands for the frequency, $\nu_0 = 215$ Hz, $S_0 = 10^{-49}\,\mathrm{Hz}^{-1}$ and ν_s is a low-frequency cut-off that can be varied and below which $S_h(\nu)$ can be considered infinite for all practical purposes (here, we choose $\nu_s = 10$ Hz).

On the other hand, a possibility for a third-generation ground-based GW detector is the ET. The basic design of this interferometer is still under discussion, so there exist some possible sensitivity curves[1] (Hild, Chelkowski & Freise 2008; Hild et al. 2010; Punturo et al. 2010a,b; Sathyaprakash et al. 2012).

Table 2. The main characteristics of the NS–NS models and their respective S/N values for a pair of 'advanced LIGOs' and ET in triangular configuration. The integration time is $T = 1$ yr. We also show the redshift z_{DC} at which the duty cycle becomes equal to 1 (transition between the popcorn and the continuous stochastic regime).

NS–NS	$\Omega_{GW\max}$	ν_p (Hz)	S/N Adv. LIGO	S/N ET	z_{DC} $D = 1$
A1	3.84×10^{-9}	375	1.46	335	0.55
A2	3.11×10^{-9}	415	1.11	256	0.57
A3	3.57×10^{-9}	390	1.32	305	0.56
A4	2.70×10^{-9}	446	0.92	211	0.61
A5	2.27×10^{-9}	485	0.71	168	0.64
A6	2.53×10^{-9}	461	0.84	194	0.62
A7	2.34×10^{-9}	482	0.76	174	0.64
A8	2.00×10^{-9}	521	0.61	142	0.67
A9	2.21×10^{-9}	498	0.70	161	0.65

Here, we use the ET-B sensitivity curve of Hild et al. (2008) with an analytical fit taken from Mishra et al. (2010):

$$S_h(\nu) = S_0 \left[a_1 x^{b_1} + a_2 x^{b_2} + a_3 x^{b_3} + a_4 x^{b_4}\right]^2 \quad \text{if } \nu \geq \nu_s$$
$$= \infty \quad \text{if } \nu < \nu_s, \quad (37)$$

where $x = \nu/\nu_0$, ν stands for the frequency, $\nu_0 = 100$ Hz, $S_0 = 10^{-50}\,\mathrm{Hz}^{-1}$ and ν_s is a low-frequency cut-off that can be varied and below which $S_h(\nu)$ can be considered infinite for all practical purposes (here, we choose $\nu_s = 10$ Hz). The coefficients in equation (37) have the values

$$\begin{aligned} a_1 &= 2.39 \times 10^{-27}, & b_1 &= -15.64, \\ a_2 &= 0.349, & b_2 &= -2.145, \\ a_3 &= 1.76, & b_3 &= -0.12, \\ a_4 &= 0.409, & b_4 &= 1.10. \end{aligned} \quad (38)$$

We consider that the ET has a triangular configuration (Hild et al. 2010) with an overlap reduction function given by Regimbau (2011). In Tables 2–4, we summarize the main characteristics of the models. We show the values of the maximum amplitude ($\Omega_{GW_{max}}$) of the stochastic background, the frequency (ν_p) where Ω_{GW} peaks and the S/N values for advanced LIGO and ET interferometers. Note that for all kinds of compact binaries we have S/N $\lesssim 1$ for a pair of advanced LIGOs. On the other hand, for ET in triangular configuration it should be possible, in principle, to obtain high values of S/N.

Concerning the nature of the GW background, it is determined by the duty cycle, which is defined as the ratio, in the observer frame, of the typical duration of a single burst $\bar{\tau}$ to the average time interval between successive events (see Regimbau & de Freitas Pacheco 2006; Regimbau & Hughes 2009):

$$D(z) = \int_0^z \bar{\tau} \frac{\mathrm{d}R_c^0}{\mathrm{d}z'} \mathrm{d}z', \quad (39)$$

where

$$\bar{\tau} = \frac{5c^5}{256\pi^{8/3} G^{5/3}} \left[\left(1 + z'\right) m_c\right]^{-5/3} f_L^{-8/3}, \quad (40)$$

[1] See also http://www.et-gw.eu/etsensitivities. In particular, the ET-C and ET-D sensitivity curves correspond to a xylophone configuration consisting of a pair of detectors. The first detector operates at low frequency (1–100 Hz) and the second one operates at high frequency (100– ~ 10 kHz).

Table 3. The main characteristics of the NS–BH models and their respective S/N values for a pair of 'advanced LIGOs' and ET in triangular configuration. The integration time is $T = 1$ yr. We also show the redshift z_{DC} at which the duty cycle becomes equal to 0.1 (transition between the shot noise and the popcorn regime).

NS–BH	Ω_{GWmax}	ν_p (Hz)	S/N Adv. LIGO	S/N ET	z_{DC} $D = 0.1$
A1	6.53×10^{-10}	123	0.52	116	0.93
A2	5.25×10^{-10}	136	0.40	88	0.99
A3	6.06×10^{-10}	128	0.47	105	0.94
A4	4.53×10^{-10}	146	0.33	73	1.15
A5	3.79×10^{-10}	159	0.26	58	1.28
A6	4.25×10^{-10}	151	0.30	67	1.19
A7	3.92×10^{-10}	158	0.27	61	1.30
A8	3.35×10^{-10}	172	0.22	49	1.51
A9	3.69×10^{-10}	164	0.25	56	1.37

Table 4. The main characteristics of the BH–BH models and their respective S/N values for a pair of 'advanced LIGOs' and ET in triangular configuration. The integration time is $T = 1$ yr.

BH–BH	Ω_{GWmax}	ν_p (Hz)	S/N Adv. LIGO	S/N ET
A1	1.68×10^{-10}	81	0.17	36
A2	1.40×10^{-10}	89	0.14	29
A3	1.58×10^{-10}	84	0.16	33
A4	1.21×10^{-10}	96	0.11	24
A5	1.04×10^{-10}	103	0.09	20
A6	1.14×10^{-10}	99	0.10	22
A7	1.06×10^{-10}	103	0.09	20
A8	9.21×10^{-11}	110	0.08	17
A9	1.00×10^{-10}	106	0.09	19

with f_L being the lower frequency bound of the detector, and m_c represents the chirp mass which is given by

$$m_c = \frac{(m_1 m_2)^{3/5}}{(m_1 + m_2)^{1/5}}. \quad (41)$$

Fig. 8 presents $D(z)$ for the NS–NS binaries, while Fig. 9 shows the duty cycle for NS–BH systems. In Fig. 10, we have the duty cycle for BH–BH systems. In these plots, we have considered $f_L = 10$ Hz.

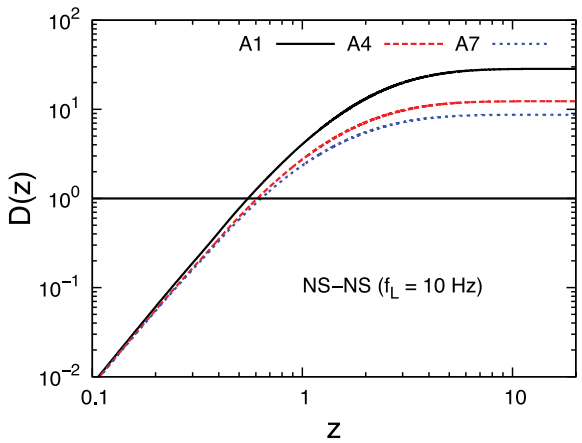

Figure 8. Duty cycle as a function of redshift for NS–NS binaries. We consider $f_L = 10$ Hz. The horizontal line at $D(z) = 1$ represents the transition between the popcorn regime and the continuous stochastic background.

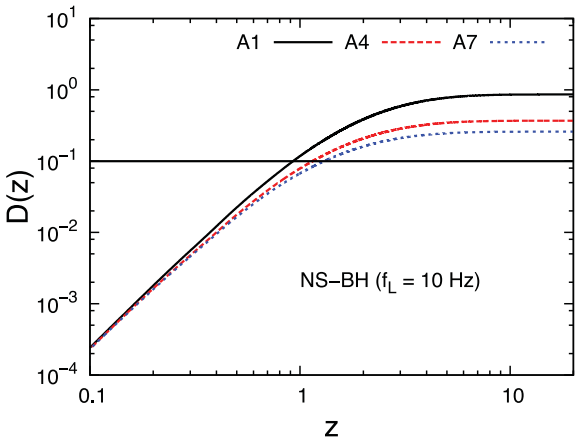

Figure 9. Duty cycle as a function of redshift for NS–BH binaries. We consider $f_L = 10$ Hz. The horizontal line at $D(z) = 0.1$ represents the transition between the shot noise and the popcorn regime.

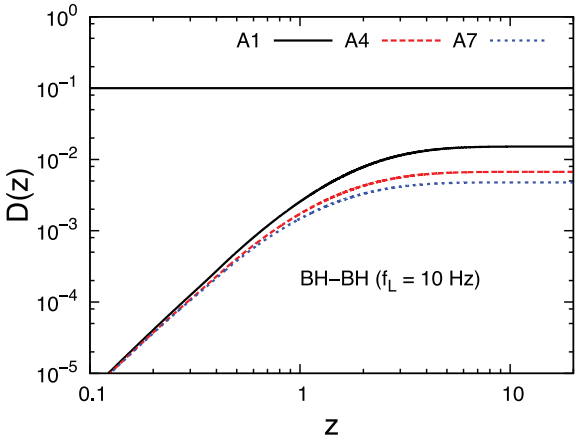

Figure 10. Duty cycle as a function of redshift for BH–BH binaries. We consider $f_L = 10$ Hz. These compact binaries produce a signal of the kind shot noise.

Concerning the duty cycle, there are three different regimes for this parameter (see e.g. Rosado 2011; Regimbau et al. 2012; Wu et al. 2012). The first case appears when $D(z) < 0.1$. In this case, we have the so-called 'shot noise regime' consisting of a sequence of widely spaced events. This means the sources can be resolved individually.

The second case appears when $0.1 < D(z) < 1$. We have the 'popcorn noise regime' in this case. This means the time interval between two successive events could be closer to the duration of a single event. In reality, near to $D(z) = 1$ the events may overlap, making it difficult to identify individual events.

The third case appears when $D(z) \geq 1$. In this case, we have a 'continuous background'. The signals overlap to produce a continuous stochastic background.

In Table 2, we include the value of the redshift z_{DC} at which the background becomes continuous [$D(z) > 1$]. In Table 3, we present the redshift of transition between the shot noise and the popcorn regime [$D(z) > 0.1$]. In particular, for NS–NS binaries a continuous background is established for sources situated at cosmological distances $z \sim 0.5$–0.6 ($z \sim 0.6$–0.7) for the cosmological-constant (Chaplygin gas) cosmology.

On the other hand, for the NS–BH binaries the signals change from shot noise to popcorn regime at $z \sim 0.9$–1.0 ($z \sim 1.0$–1.5

for Chaplygin gas). For the BH–BH systems, the signals are always within the shot noise regime. However, note that reducing the values of the local merger $\dot{\rho}_c^0(0)$ in relation to those values used in the present work would reduce the values of the S/N besides changing the regimes [or values of $D(z)$] of the GW backgrounds. In particular, note that S/N and $D(z)$ are proportional to $\dot{\rho}_c^0(0)$.

4.2 Collapse of stars to form black holes

In order to determine the background of GWs generated by stars which collapse to black holes, we rewrite equation (30) as

$$F_{\nu_{\rm obs}} = \int_0^{z_{\rm ini}} f_{\nu_{\rm obs}}\, {\rm d}R_{\rm BH}(z), \tag{42}$$

where now we have

$$\frac{{\rm d}R_{\rm BH}}{{\rm d}z} = \dot{\rho}_\star(z)\Phi(m)\,{\rm d}m\frac{{\rm d}V}{{\rm d}z}, \tag{43}$$

and for $f_{\nu_{\rm obs}}$ we have

$$f_{\nu_{\rm obs}} = \frac{\pi c^3}{2G}h_{\rm BH}^2. \tag{44}$$

The dimensionless amplitude $h_{\rm BH}$ is given by (Thorne 1987)

$$h_{\rm BH} \simeq 7.4\times10^{-20}\varepsilon_{\rm GW}^{1/2}\left(\frac{m_{\rm r}}{{\rm M}_\odot}\right)\left(\frac{d_{\rm L}}{1\,{\rm Mpc}}\right)^{-1}, \tag{45}$$

where $\varepsilon_{\rm GW}$ is the efficiency of generation of GWs and $m_{\rm r}$ is the mass of the black hole formed.

It is worth mentioning that equation (45) refers to the black hole 'ringing', which has to do with the de-excitation of the black hole quasi-normal modes.

The collapse of a star to black hole produces a signal with frequency $\nu_{\rm obs}$ given by

$$\nu_{\rm obs} \simeq 1.3\times10^4{\rm Hz}\left(\frac{{\rm M}_\odot}{m_{\rm r}}\right)(1+z)^{-1}. \tag{46}$$

We will consider that black holes are formed from stars with $40 \le m \le 140\,{\rm M}_\odot$. The lower limit is consistent with recent results derived from the X-ray pulsar CXO J164710.2−455216, which shows that the progenitor to this pulsar had an initial mass $\sim$40 $\rm M_\odot$ (Muno et al. 2006). On the other hand, the mass of the black hole remnant is taken to be the mass of the helium core before collapse (see Heger & Woosley 2002). Thus,

$$m_{\rm r} = m_{\rm He} = \frac{13}{24}(m - 20\,{\rm M}_\odot). \tag{47}$$

With these considerations, we can obtain the spectrum of GWs produced by cosmological black holes. Fig. 11 shows the spectrum of the gravitational energy density parameter $\Omega_{\rm GW}$ as a function of the observed frequency $\nu_{\rm obs}$ for the models with the highest S/N of Table 5. These curves consider $\varepsilon_{\rm GW} = 10^{-4}$ (Löffler, Rezzolla & Ansorg 2006).

We can see that the spectra peak at $\Omega_{\rm GW} \sim 3\times10^{-9}$ to 10^{-7}, which is dependent on both CSFR parameters and dark energy component. Note that only two models have transition from shot noise to popcorn regime (which corresponds to $D = 0.1$). All the other models correspond to shot noise signals.

Fig. 12 presents the duty cycle generated by the collapse of stars to form black holes. Note that in this case we calculate the duty cycle as

$$D(z) = \int_0^z \bar{\tau}(1+z')\frac{{\rm d}R_{\rm BH}}{{\rm d}z'}{\rm d}z', \tag{48}$$

with $\bar{\tau} = 1$ ms (Ferrari et al. 1999).

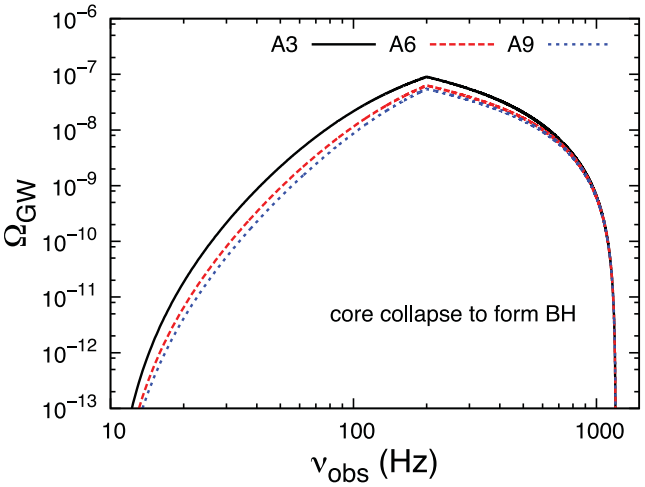

Figure 11. Spectrum of the gravitational energy density parameter $\Omega_{\rm GW}$. We consider an efficiency of generation of GWs, $\varepsilon_{\rm GW} = 10^{-4}$.

Table 5. The main characteristics of the models 'core-collapse to form black holes'. The efficiency of generation of GWs is $\varepsilon_{\rm GW} = 10^{-4}$. The S/N values for a pair of 'advanced LIGO' are determined for an integration time $T = 1$ yr. For ET we consider triangular configuration. We also show the redshift $z_{\rm DC}$ at which the duty cycle becomes equal to 0.1 (transition from shot noise to popcorn regime).

BH	$\Omega_{\rm GWmax}$	$\nu_{\rm p}$ (Hz)	S/N Adv. LIGO	S/N ET	$z_{\rm DC}$ $D = 0.1$
A1	6.80×10^{-9}	200	0.14	152	–
A2	5.00×10^{-9}	200	0.08	96	–
A3	9.02×10^{-8}	200	1.76	1900	3.38
A4	4.70×10^{-9}	200	0.07	86	–
A5	3.63×10^{-9}	200	0.04	58	–
A6	6.29×10^{-8}	200	0.85	1100	6.92
A7	4.06×10^{-9}	200	0.05	68	–
A8	3.20×10^{-9}	200	0.03	48	–
A9	5.46×10^{-8}	200	0.62	870	–

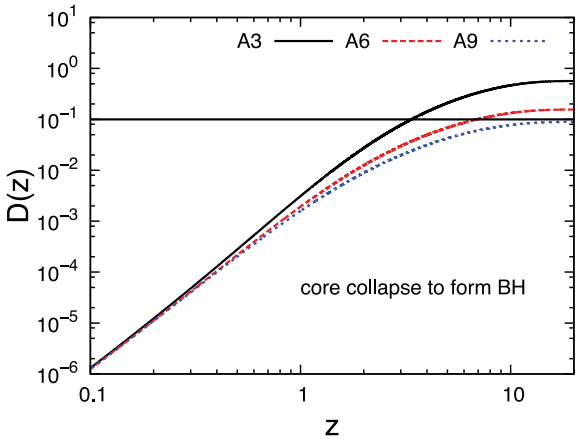

Figure 12. Duty cycle as a function of redshift for the cosmological population of black holes. The horizontal line at $D(z) = 0.1$ represents the transition from shot noise to popcorn regime.

We can observe from Table 5 that the frequency where the spectra peak depends neither on the dark energy cosmology nor on the CSFR parameters. Another characteristic of this kind of source is the very high S/N produced for ET.

It is worth stressing that Zhu, Howell & Blair (2010) have recently estimated the upper limit on the energy density, of a stochastic GW background, produced by the core-collapse SNe leaving black holes as remnants. The authors showed that by considering Gaussian source spectra it would be possible to detect GW signals with $\varepsilon_{\rm GW} \sim 10^{-5}\,(10^{-7})$ for advanced LIGO (ET). Another work centred on the GW backgrounds produced by core-collapse SNe of Population III and Population II stars was developed by Marassi, Schneider & Ferrari (2009). In particular, the authors studied the cosmic transition of Population III to Population II using waveforms derived from recent 2D numerical simulations. The GW efficiencies used by these authors were $\varepsilon_{\rm GW} \sim 10^{-7}$ for Population II progenitors and $\varepsilon_{\rm GW} \sim 10^{-5}$ for Population III progenitors (with initial masses ranging between 100 and 500 $\rm M_{\odot}$). Here, we have adopted the GW spectrum of Thorne (1987), with efficiency $\varepsilon_{\rm GW} \sim 10^{-4}$, because the core-collapse energy spectrum will affect the results for both cases, ΛCDM and Chaplygin gas, exactly the same way.

5 COSMOLOGICAL SPECTRUM PRODUCED BY ALL SOURCES

It is worth stressing that a stochastic background of GWs is expected to arise from a superposition of a large number of GW sources of astrophysical and cosmological origin. In particular, the *Wilkinson Microwave Anisotropy Probe* (*WMAP*) results suggest an early epoch for the reionization of the Universe (see e.g. Jarosik et al. 2011). In this way, a pre-galactic population should be formed at high redshifts to account for these results. The cosmic star formation history is determined by the interplay between the incorporation of baryons into collapsed objects and return of baryons into diffuse state (e.g. gaseous clouds).

Thus, the formation of different objects such as NS–NS binaries, NS–BH binaries, BH–BH systems and core-collapse SNe to form black holes, among others, is directly related to the CSFR. On the other hand, different dark energy scenarios could give different signatures on the background through the expansion function $E(z)$ (equation 6). As the GW background could trace the behaviour of the Universe up to redshift ∼20, it should be possible to infer if there is a temporal dependence of the dark energy equation of state, i.e. if $\dot{w}(a) \neq 0$.

In this way, the detection and characterization of a stochastic background of GWs could be used as a tool for the study of the Universe at high redshifts. In particular, the GW signals produced at different cosmological distances by the sources discussed above could overlap at a given frequency $\nu_{\rm obs}$ to produce a stochastic background over a large range in frequency.

In Fig. 13, we show the collective contribution of the three compact binary sources investigated here. In Table 6, we summarize the main characteristics of these models. Although the S/N of the collective spectra are dominated by the NS–NS binaries, we note that the NS–BH and BH–BH binaries pull the peak of the collective spectra for lower frequencies than those observed if we only consider the NS–NS systems.

In Fig. 14, we include the core-collapse SNe together with the compact binary systems in the calculation of the GW spectra. We can see that for a low efficiency of generation of GWs ($\varepsilon_{\rm GW} = 10^{-4}$) the collective spectra show a clear signature of this kind of source when compared to the spectra derived only with compact binaries.

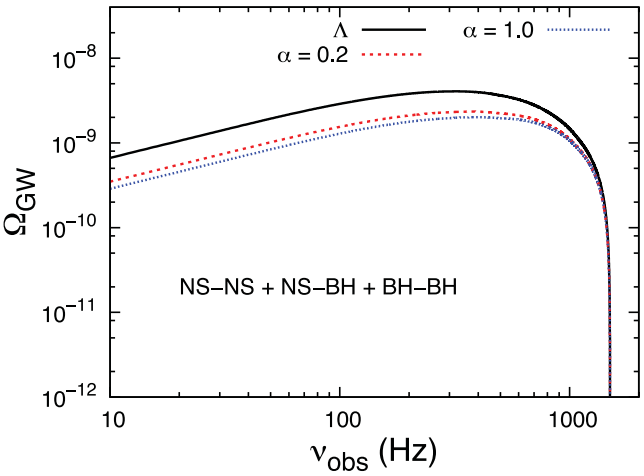

Figure 13. Collective spectra of the three compact binary sources studied in this work. The curves represent the models A1, A4 and A7.

Table 6. The main characteristics of the collective contribution of the three compact binary sources, namely NS–NS binaries, NS–BH systems and BH–BH binaries. The S/N values for a pair of 'advanced LIGO' are determined for an integration time $T = 1$ yr. We also present the S/N for ET in triangular configuration.

Model	$\Omega_{\rm GWmax}$	$\nu_{\rm p}$ (Hz)	S/N Adv. LIGO	S/N ET
A1	4.06×10^{-9}	321	2.15	486
A2	3.27×10^{-9}	346	1.64	373
A3	3.77×10^{-9}	331	1.95	442
A4	2.81×10^{-9}	374	1.35	308
A5	2.34×10^{-9}	398	1.08	246
A6	2.63×10^{-9}	385	1.24	283
A7	2.42×10^{-9}	396	1.12	254
A8	2.04×10^{-9}	413	0.91	207
A9	2.27×10^{-9}	404	1.03	235

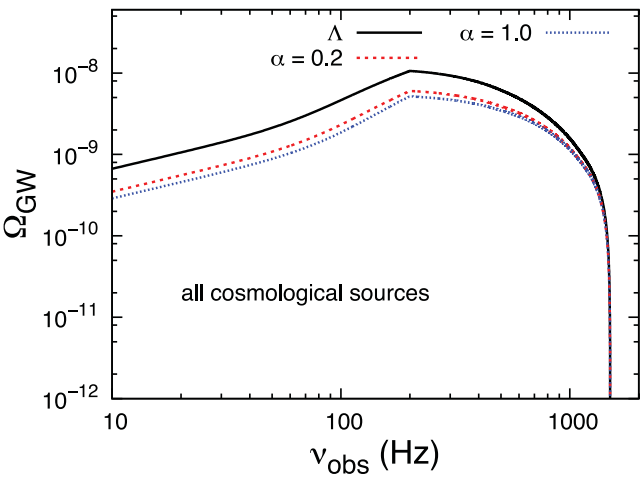

Figure 14. Spectrum of all sources studied in this work. Concerning the core-collapse SNe to form black holes, we use $\varepsilon_{\rm GW} = 10^{-4}$. The curves represent the models A1, A4 and A7.

Table 7. The main characteristics of the collective contribution of all sources studied in this work. The S/N values for a pair of 'advanced LIGO' are determined for an integration time $T = 1$ yr. We also present the S/N for ET in triangular configuration.

Model	$\Omega_{\rm GWmax}$	$\nu_{\rm p}$ (Hz)	S/N Adv. LIGO	S/N ET
A1	1.06×10^{-8}	200	2.23	590
A2	8.00×10^{-9}	200	1.69	433
A3	9.36×10^{-8}	200	3.26	2182
A4	7.23×10^{-9}	200	1.39	362
A5	5.69×10^{-9}	200	1.10	280
A6	6.52×10^{-8}	200	1.81	1262
A7	6.19×10^{-9}	200	1.14	295
A8	4.96×10^{-9}	200	0.92	233
A9	5.65×10^{-8}	200	1.42	1005

In Table 7 we present the main characteristics of the collective spectra for all sources studied in this work.

We note that core-collapse SNe have an important contribution for the shape of the collective spectrum for frequencies in the range 60 – ∼300 Hz. In particular, the frequency where the collective spectra peak is completely dominated by the core-collapse SNe. Note that model A3 could produce S/N ∼ 3 (∼2200) for advanced LIGO (ET) in the cosmological-constant cosmology. On the other hand, model A6 could produce S/N ∼ 2 (∼1300) for advanced LIGO (ET) in the Chaplygin gas cosmology. In principle, detecting stochastic backgrounds of GWs with high S/N could make the inference of, for example, the behaviour of the CSFR at high redshifts as well as any temporal dependence of the dark energy equation of state possible.

6 COMPACT BINARIES AND CORE-COLLAPSE PARAMETERS: INFLUENCE ON THE RESULTS

In the previous sections, we have analysed the main characteristics of the stochastic backgrounds produced by compact binary systems, core-collapse to form black holes and the composite signal of these cosmological objects. We verify that higher S/N values can be produced if we consider ET in triangular configuration. Although these cosmological sources are connected by the CSFR, we know that there are uncertainties in the minimum coalescence time-scales of NS–NS, NS–BH and BH–BH binaries. On the other hand, the local coalescence rates of these systems can vary by up to three orders of magnitude. In addition, the minimum mass able to form a black hole may vary from ∼25 $M_\odot$ to ∼40 $M_\odot$. Thus, in this section, we present an analysis of these uncertainties and their influence on the stochastic backgrounds discussed here. We also discuss if there is a clear difference between the ΛCDM and the Chaplygin gas which would permit us to constrain both the constant feature (or not) of the dark energy equation of state and the CSFR derived for ΛCDM and Chaplygin gas. In particular, we have analysed the following.

(a) *The local coalescence rate*. This parameter acts like an offset and it does not modify the shapes of the spectra. Note, however, that $S/N \propto \dot{\rho}_{\rm c}^0(0)$ and so our S/N values can vary from 0.1 to 10 of those listed in Tables 2–4. Thus, this parameter can only modify the values of the S/N as $S/N = \dot{\rho}_{\rm c}^0(0)/\dot{\rho}_{\rm c}^0(0)_{\rm u} \times (S/N)_{\rm u}$, where the subscript u means the values used and derived in this work. Note that in the worst case $[\dot{\rho}_{\rm c}^0(0) = 0.1 \times \dot{\rho}_{\rm c}^0(0)_{\rm u}]$, it would be possible to have S/N > 10 (ET) for the composite signals of these three binary sources. Concerning the duty cycle, observe that $D(z)$ is also proportional to $\dot{\rho}_{\rm c}^0(0)$. Thus, the redshifts of transition from popcorn to continuous regimes (and from shot noise to popcorn regimes) can change according to the values of $\dot{\rho}_{\rm c}^0(0)$.

(b) *The minimum stellar mass to form a black hole*. This parameter basically changes the maximum frequency of the background formed by core-collapse. In the case $m_{\rm min} = 25\,M_\odot$, we obtain $\nu_{\rm max} = 4.8$ kHz, while for $m_{\rm min} = 40\,M_\odot$ we have $\nu_{\rm max} = 1.2$ kHz. In terms of S/N, if we change $m_{\rm min}$ from 40 to 25 $M_\odot$, the S/N values increase by 5 per cent in relation to those values present in Table 5. Looking at the results in Table 7, collective contribution of all sources, S/N increases by 2 per cent (50 per cent) for advanced LIGO (ET). The frequency where $\Omega_{\rm GW}$ peaks is weakly dependent on this parameter in both ΛCDM and Chaplygin gas cases.

(c) *Efficiency of generation of GWs (ε_{GW})*. Note that $\Omega_{\rm GW} \propto \varepsilon_{\rm GW}$. Thus, with an efficiency of generation of GWs $\sim 10^{-5}$ to 10^{-6}, it could be possible to have S/N > 10 for ET in triangular configuration (see Table 5).

(d) *Coalescence time-scale of NS–NS*. We change this parameter from 20 to 100 Myr. As a consequence, the coalescence rate peaks at $z \sim 1.9\,(1.30)$ instead of at $z \sim 2.27\,(1.63)$ for the ΛCDM (Chaplygin gas with $\alpha = 0.2$), while the S/N of Table 2 typically decreases by 15 per cent. Looking at the collective contribution of all sources in Table 7, we note that S/N decreases by 8 per cent (3 per cent) for advanced LIGO (ET). There is just a slight modification of the frequency where $\Omega_{\rm GW}$ peaks.

(e) *Coalescence time-scale of NS–BH*. We change this parameter from 10 to 50 Myr. As a consequence, the coalescence rate peaks at $z \sim 2.1\,(1.50)$ instead of at $z \sim 2.45\,(1.81)$ for the ΛCDM (Chaplygin gas with $\alpha = 0.2$), while the S/N of Table 3 typically decreases by 10 per cent. Looking at the collective contribution of all sources in Table 7, we note that S/N decreases by 1 per cent for both advanced LIGO and ET.

(f) *Coalescence time-scale of BH–BH*. We change this parameter from 100 to 500 Myr. As a consequence, the coalescence rate peaks at $z \sim 1.25\,(0.83)$ instead of at $z \sim 1.86\,(1.31)$ for the ΛCDM (Chaplygin gas with $\alpha = 0.2$), while the S/N of Table 4 typically decreases by 20 per cent. Looking at the collective contribution of all sources in Table 7, we note that S/N decreases by 0.8 per cent for both advanced LIGO and ET.

A question could arise about the uncertainties described above: is it possible to have a clear separation of the two backgrounds (ΛCDM and Chaplygin gas cosmologies) or the uncertainties listed above produce a superposition of these backgrounds? A second question could also arise: can different dark energy scenarios produce distinct signatures on the CSFR? In order to answer these questions, we present in Figs 15 and 16 the GW backgrounds with the uncertainties discussed above and for models A1 and A4 of Table 1. In these figures, we just keep two parameters fixed: $\varepsilon_{\rm GW} = 10^{-4}$ and $m_{\rm min} = 40\,M_\odot$. Below $\nu_{\rm obs} \sim 1$ kHz, there is no superposition between the GW signals in the case of ΛCDM and Chaplygin gas ($\alpha = 0.2$), with all the uncertainties in the parameters. However, note that the case of Chaplygin gas with $\alpha = 1$ cannot be separated from that with $\alpha = 0.2$. There is a superposition between these two Chaplygin models if we take into account all the uncertainties discussed above.

The second point is related to the CSFR. Looking at Fig. 17, we see that there is no overlap between the cases ΛCDM and Chaplygin gas at $z > 2$, with all the uncertainties in the parameters. The areas defined by ΛCDM and Chaplygin gas cosmology do not overlap in

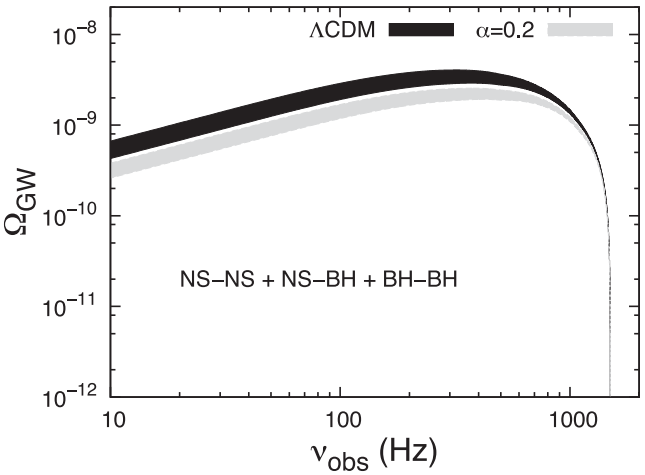

Figure 15. Collective spectra of the three compact binaries taking into account the uncertainties in the parameters. The black area describes all the possible GW signals for the ΛCDM case. The grey area represents the GW backgrounds for Chaplygin gas with $\alpha = 0.2$.

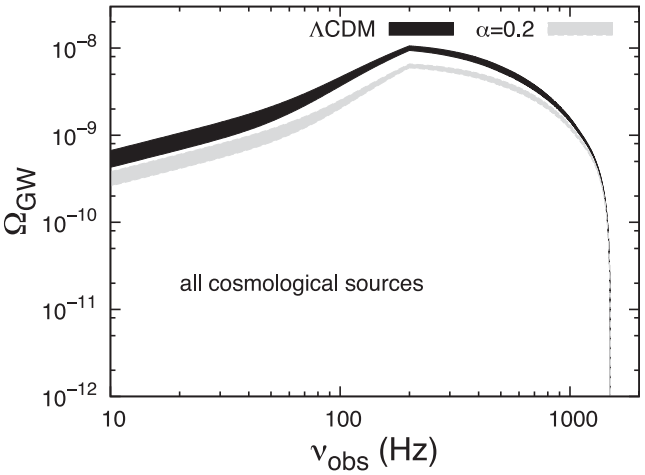

Figure 16. Collective spectra of all sources studied in this work taking into account the uncertainties in the parameters. The black area describes all the possible GW signals for the ΛCDM case. The grey area represents the GW backgrounds for Chaplygin gas with $\alpha = 0.2$.

the redshift range [2–20]. In principle, with observational data less scattered in the range $z \sim 2$–5, it would be possible to have a better indication of the dark energy equation of state from the observed CSFR. Otherwise, a stochastic background of GWs with high S/N being detected, as in the case of ET, we could work with the inverse problem reconstructing the CSFR from the observed background. In this way, ET could contribute for a better comprehension of how star formation is regulated at high redshifts.

7 FINAL REMARKS

In this work, we have first studied the main characteristics of the GW signals produced by coalescences of NS–NS, NS–BH and BH–BH binaries up to redshift $z \sim 20$. The coalescence rates are obtained from the hierarchical formation scenario recently studied by Pereira & Miranda (2010).

In this formalism, the 'CSFR' is derived in a self-consistent way, considering the baryon accretion rate as an infall term which supplies the gaseous reservoir in the haloes. However, here we modify

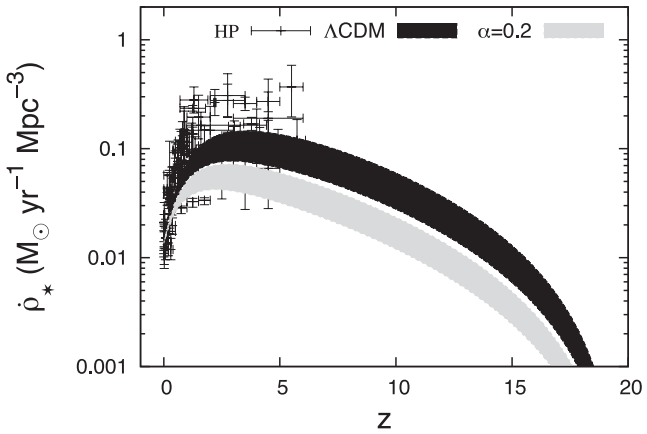

Figure 17. Possible CSFRs taking into account all the viable models studied in this work. The black area represents the family of CSFRs for the ΛCDM cosmology (models A1 to A3), while the grey area shows the family of CSFRs for the Chaplygin gas (models A4 to A6) as dark energy component of the Universe. Note that there is no overlap at $z > 2$ between these two dark fluids, with all the uncertainties in the parameters.

their model in order to incorporate different dark energy fluids. In particular, we show results considering two different dark energy components of the Universe: the cosmological constant and the Chaplygin gas.

For NS–NS systems, the shape of the spectrum of the gravitational energy density parameter ($\Omega_{\rm GW}$) has a good agreement with the case studied by Regimbau & de Freitas Pacheco (2006), who used numerical simulations based on Monte Carlo methods. In particular, we have obtained S/N $\sim$ 1.5 for NS–NS, S/N $\sim$ 0.50 for NS–BH and S/N $\sim$ 0.20 for BH–BH binaries in the cosmological-constant cosmology and considering the correlation of two advanced LIGO detectors. If we consider ET in triangular configuration, the S/N values are at least a factor of $\sim$200 greater than those obtained for advanced LIGO. The signals produced in the case of Chaplygin gas are always lower than those produced by the cosmological-constant cosmology.

We have also analysed the nature of the GW background produced by those compact binaries. For our fiducial parameters, we verify that a continuous background, corresponding to a duty cycle $\gtrsim$1, is produced by sources situated at cosmological distances far from $z \sim 0.5$–0.6 for NS–NS binaries in the cosmological-constant cosmology. For the Chaplygin gas cosmology, duty cycle $\gtrsim$1 is obtained for sources far from $z \sim 0.6$–0.7.

Considering NS–BH binaries, the nature of the background becomes popcorn for sources far from $z \sim 0.9$–1.0 ($z \sim 1.0$–1.5) if the dark component of the Universe is the cosmological constant (Chaplygin gas). On the other hand, BH–BH binaries are always within the shot noise regime.

We also verify the characteristics of the background produced by a cosmological population of stellar core-collapse SNe to form black holes. In this case, S/N values within the range from $\sim$0.05 to $\sim$2 could be generated depending upon the CSFR/dark energy component and the efficiency of generation of GWs used. We verify that this population does not behave as a continuous background. However, for sources situated at cosmological distances $z \sim 3$ ($z \sim 7$) we verify a transition from shot noise to popcorn regime if the time-scale for star formation ($\tau_{\rm s}$) is $\sim$1 Gyr and if the dark energy component is the cosmological constant (Chaplygin gas).

A stochastic background of GWs, from cosmological origin, is expected to arise from a superposition of different GW sources at

different redshifts. In particular, the formation of different objects such as NS–NS binaries, NS–BH binaries, BH–BH systems and core-collapse SNe to form black holes, among others, is related to the CSFR. In this way, we determine the shape of a pre-galactic background of GWs considering the collective effect of these different objects. We obtain that a stochastic background of GWs could be generated in the range of frequency 10 Hz–1.5 kHz with an S/N $\sim$3 ($\sim$2) for a pair of advanced LIGO interferometers and if the dark energy component is the cosmological constant (Chaplygin gas).

It is worth stressing that the sensitivity of the future third-generation detectors, for example the ET, could be high enough to increase the expected values of S/N. For example, if we consider the ET-B sensitivity curve in triangular configuration, the gain in relation to advanced LIGO would be $\sim$300–1000. Thus, instruments such as ET could permit us to explore the epoch when the first stars were formed in the Universe at the end of the so-called 'dark ages'. In this way, the detection and characterization of a stochastic background of GWs, over a large range in frequency, could be used as a tool for the study of the star formation up to redshift $z \sim 20$.

Recently, Marassi et al. (2009, 2011b) also have analysed stochastic backgrounds of GWs but with a CSFR derived by Tornatore, Ferrara & Schneider (2007), which includes sources up to $z \sim 15$. Comparing the results of those papers with Fig. 1 of the present work, for the ΛCDM case, we note that both CSFRs produce similar results up to $z \sim 3$. At higher redshifts ($z > 3$), the present study predicts more sources than the Tornatore–Ferrara–Schneider CSFR (TFS-CSFR). This happens because Pereira & Miranda model (PM-CSFR) incorporates more baryons in stars than TFS-CSFR.

The preference for using PM-CSFR comes from the following points. (a) The dark energy component, with an equation of state dependent on time, modifies both the expansion factor $E(z)$ and the growth function (see equations 2 and 8). TFS-CSFR uses the GADGET code with the ΛCDM model as the background cosmology. Thus, it would not be possible for TFS-CSFR to study consistently the case of Chaplygin gas as dark energy fluid. This means that we would not have to compare their results with those obtained here for the case of Chaplygin gas.

Note that one of our results was to show that the dark energy component modifies the amplitude of the CSFR. (b) Recently, Pereira & Miranda (2011) studied four different CSFRs (Springel & Hernquist 2003; Hopkins & Beacom 2006; Fardal et al. 2007; Pereira & Miranda 2010) to derive the evolution of the comoving black hole mass density. Their results show that PM-CSFR has a good agreement with the quasar luminosity density up to redshift $\sim$6. On the other hand, as PM-CSFR produces a high number of sources at $z > 3$, there exist an important contribution of these objects, formed at high redshifts, to the backgrounds studied in the present paper. This is an intrinsic characteristic of the scenario used by Pereira & Miranda (2010) to derive the CSFR.

As a final point, different dark energy scenarios could give different signatures on the background through the expansion function $E(z)$. As the GW background could trace the behaviour of the Universe up to redshift $\sim$20, in principle it should be possible to infer if there is a temporal dependence of the dark energy equation of state, i.e. if $\dot{w}(a) \neq 0$. In this way, not only binary systems at lower redshifts ($z < 2$–3) working as standard sirens (e.g. Sathyaprakash, Schutz & Van Den Broeck 2010; Zhao et al. 2011) but also stochastic backgrounds of GWs could contribute for a better comprehension of the physical nature of the dark energy. We observe that all viable dark energy fluids have similar behaviour up to $z \sim 1.5$ where the main observational data are available (e.g. SNIa and baryon acoustic oscillations). This fact can be inferred from the CSFR (see Fig. 1), where for $z < 2$ all models (cosmological constant and Chaplygin gas) have similar evolution. Thus, a way to identify if $\dot{w}(a) \neq 0$ would be to observe the Universe at higher redshifts. In principle, stochastic backgrounds of GWs could be such observable.

ACKNOWLEDGMENTS

ODM would like to thank the Brazilian Agency CNPq for partial financial support (grant 300713/2009-6). The author would like to thank the referee, Tania Regimbau, for helpful comments that considerably improved the paper.

REFERENCES

Abbott B. P. et al., 2009, Rep. Progress Phys., 72, 076901
Acernese F. et al., 2008, Class. Quantum Grav., 25, 184001
Aguiar O. D. et al., 2008, Class. Quantum Grav., 25, 114042
Albrecht A., Skordis C., 2000, Phys. Rev. Lett., 84, 2076
Allen B., 1997, in Marck J.-A., Lasota J.-P., eds, Relativistic Gravitation and Gravitational Radiation. Cambridge Univ. Press, Princeton, NJ, p. 373
Allen B., Romano J. D., 1999, Phys. Rev. D, 59, 102001
Alves M. E. S., Miranda O. D., de Araujo J. C. N., 2009, Phys. Lett. B, 679, 401
Amaro-Seoane P. et al., 2012, Class. Quantum Grav., 29, 124016
Ando M. et al., 2010, Class. Quantum Grav., 27, 084010
Belczyński K., Kalogera V., Bulik T., 2002, ApJ, 572, 407
Bento M. C., Bertolami O., Santos N. C., 2002, Phys. Rev. D, 65, 067301
Bordemann M., Hoppe J., 1994, Phys. Lett. B, 325, 359
Bulik T., Belczyński K., Rudak B., 2004, A&A, 415, 407
Christensen N., 1992, Phys. Rev. D, 46, 5250
Christensen C. R., Quinn T., Stinson G., Bellovary J., Wadsley J., 2010, ApJ, 717, 121
Colistete R., Jr, Fabris J. C., 2005, Class. Quantum Grav., 22, 2813
Copi C. J., 1997, ApJ, 487, 704
Cutler C., Harms J., 2006, Phys. Rev. D, 73, 042001
Daigne F., Olive K. A., Silk J., Stoehr F., Vangioni E., 2006, ApJ, 647, 773
de Araujo J. C. N., Miranda O. D., 2005, Phys. Rev. D, 71, 127503
de Araujo J. C. N., Miranda O. D., Aguiar O. D., 2000, Phys. Rev. D, 61, 124015
de Araujo J. C. N., Miranda O. D., Aguiar O. D., 2002, MNRAS, 330, 651
de Araujo J. C. N., Miranda O. D., Aguiar O. D., 2004, MNRAS, 348, 1373
de Freitas Pacheco J. A., 1997, Astropart. Phys., 8, 21
de Freitas Pacheco J. A., Regimbau T., Spallici A., Vincent S., 2006, Int. J. Modern Phys. D, 15, 235
de Paula W. L. S., Miranda O. D., Marinho R. M., 2004, Class. Quantum Grav., 21, 4595
Fabris J. C., Velten H. E. S., Zimdahl W., 2010, Phys. Rev. D, 81, 087303
Fardal M. A., Katz N., Weinberg D. H., Davé R., 2007, MNRAS, 379, 985
Ferrari V., Matarrese S., Schneider R., 1999, MNRAS, 303, 247
Flanagan E. E., 1993, Phys. Rev. D, 48, 2389
Giovannini M., 2010, PMC Phys. A, 4, 1
Gorini V., Moschella U., Kamenshchik A., Pasquier V., 2005, in Vilasi G., Espositio G., Lambiase G., Marmo G., Scarpetta G., eds., AIP Conf.AIP Conf. Proc. Vol. 751, General Relativity and Gravitational Physics. Am. Inst. Phys., New York, p. 108
Gottardi L. et al., 2007, Phys. Rev. D, 76, 102005
Grote H. (for the LIGO Scientific Collaboration), 2008, Class. Quantum Grav., 25, 114043
Heger A., Woosley S. E., 2002, ApJ, 567, 532
Hild S., Chelkowski S., Freise A., 2008, preprint (arXiv:0810.0604)
Hild S. et al., 2011, Class. Quantum Grav., 28, 094013
Hopkins A. M., 2004, ApJ, 615, 209
Hopkins A. M., 2007, ApJ, 654, 1175
Hopkins A. M., Beacom J. F., 2006, ApJ, 651, 142
Hulse R. A., Taylor J. H., 1974, ApJ, 191, L59
Hulse R. A., Taylor J. H., 1975a, ApJ, 195, L51

Hulse R. A., Taylor J. H., 1975b, ApJ, 201, L55
Jarosik N. et al., 2011, ApJS, 192, 14
Jenkins A., Frenk C. S., White S. D. M., Colberg J. M., Cole S., Evrard A. E., Couchman H., Yoshida N., 2001, MNRAS, 321, 372
Löffler F., Rezzolla L., Ansorg M., 2006, Phys. Rev. D, 74, 104018
Lukić Z., Heitmann K., Habib S., Bashinsky S., Ricker P. M., 2007, ApJ, 671, 1160
Maggiore M., 2000, Phys. Rep., 331, 283
Marassi S., Schneider R., Ferrari V., 2009, MNRAS, 398, 293
Marassi S., Schneider R., Corvino G., Ferrari V., Portegies Zwart S., 2011a, Phys. Rev. D, 84, 124037
Marassi S., Ciolfi R., Schneider R., Stella L., Ferrari V., 2011b, MNRAS, 411, 2549
Miranda O. D., de Araujo J. C. N., Aguiar O. D., 2004, Class. Quantum Grav., 21, S557
Mishra C. K., Arun K. G., Iyer B. R., Sathyaprakash B. S., 2010, Phys. Rev. D, 82, 06010
Muno M. P. et al., 2006, ApJ, 636, L41
Neyman J., Scott E. L., Shane C. D., 1952, ApJ, 116, 144
Ogawa N., 2000, Phys. Rev. D, 62, 085023
Pace F., Waizmann J.-C., Bartelmann M., 2010, MNRAS, 406, 1865
Peacock J. A., 1999, Cosmological Physics. Cambridge Univ. Press, Cambridge, p. 682
Pereira E. S., Miranda O. D., 2010, MNRAS, 401, 1924
Pereira E. S., Miranda O. D., 2011, MNRAS, 418, L30
Peters P. C., Mathews J., 1963, Phys. Rev. D, 131, 435
Piattella O., 2010, J. Cosmol. Astropart. Phys., 1003, 012
Press W. H., Schechter P., 1974, ApJ, 193, 425
Punturo M. et al., 2010a, Class. Quantum Grav., 27, 084007
Punturo M. et al., 2010b, Class. Quantum Grav., 27, 194002
Regimbau T., 2011, Res. Astron. Astrophys., 11, 369
Regimbau T., de Freitas Pacheco J. A., 2001, A&A, 376, 381
Regimbau T., de Freitas Pacheco J. A., 2006, ApJ, 642, 455
Regimbau T., Hughes S. A., 2009, Phys. Rev. D, 79, 062002
Regimbau T. et al., 2012, preprint (arXiv:1201.3563)
Rosado P., 2011, Phys. Rev. D, 84, 084004
Sandick P., Olive K. A., Daigne F., Vangioni E., 2006, Phys. Rev. D, 73, 104024
Sathyaprakash B. S., 2001, Pramana, 56, 457
Sathyaprakash B. S., Schutz B. F., Van Den Broeck C., 2010, Class. Quantum Grav., 27, 215006
Sathyaprakash B. S. et al., 2012, Class. Quantum Grav., 29, 124013
Scalo J., 1986, Fundamentals Cosmic Phys., 11, 1
Schmidt M., 1959, ApJ, 129, 243
Schmidt M., 1963, ApJ, 137, 758
Somiya K. (for the KAGRA Collaboration), 2012, Class. Quantum Grav., 29, 124007
Springel V., Hernquist L., 2003, MNRAS, 339, 312
Suwa Y., Takiwaki T., Kotake K., Sato K., 2007, ApJ, 665, L43
Takahashi R. and the TAMA Collaboration, 2004, Class. Quantum Grav., 21, S403
Thorne K. P., 1987, in Hawking S. W., Israel W., eds, Three Hundred Years of Gravitation. Cambridge Univ. Press, Cambridge, p. 330
Tinsley B. M., 1973, ApJ, 186, 35
Tornatore L., Ferrara A., Schneider R., 2007, MNRAS, 382, 945
Wu C., Mandic V., Regimbau T., 2012, Phys. Rev. D, 85, 104024
Zhao W., Van Den Broeck C., Baskaran D., Li T. G. F., 2010, Phys. Rev. D, 83, 023005
Zhu X. J., Howell E., Blair D., 2010, MNRAS, 409, L132
Zhu X.-J., Howell E., Regimbau T., Blair D., Zhu Z.-H., 2011, ApJ, 739, 86

This paper has been typeset from a TEX/LATEX file prepared by the author.